NANO LETTERS

Subscriber access provided by King Abdullah University of Science and Technology Library

Communication

# Intercorrelated in-plane and out-of-plane ferroelectricity in ultrathin two-dimensional layered semiconductor In2Se3

Chaojie Cui, Weijin Hu, Xingxu Yan, Christopher Addiego, Wenpei Gao, Yao Wang, Zhe Wang, Linze Li, Yingchun Cheng, Peng Li, Xixiang Zhang, Husam N. Alshareef, Tom Wu, Wenguang Zhu, Xiaoqing Pan, and Lain-Jong Li

*Nano Lett.*, **Just Accepted Manuscript** • DOI: 10.1021/acs.nanolett.7b04852 • Publication Date (Web): 29 Jan 2018

**Downloaded from http://pubs.acs.org on February 5, 2018**

## Just Accepted

"Just Accepted" manuscripts have been peer-reviewed and accepted for publication. They are posted online prior to technical editing, formatting for publication and author proofing. The American Chemical Society provides "Just Accepted" as a service to the research community to expedite the dissemination of scientific material as soon as possible after acceptance. "Just Accepted" manuscripts appear in full in PDF format accompanied by an HTML abstract. "Just Accepted" manuscripts have been fully peer reviewed, but should not be considered the official version of record. They are citable by the Digital Object Identifier (DOI®). "Just Accepted" is an optional service offered to authors. Therefore, the "Just Accepted" Web site may not include all articles that will be published in the journal. After a manuscript is technically edited and formatted, it will be removed from the "Just Accepted" Web site and published as an ASAP article. Note that technical editing may introduce minor changes to the manuscript text and/or graphics which could affect content, and all legal disclaimers and ethical guidelines that apply to the journal pertain. ACS cannot be held responsible for errors or consequences arising from the use of information contained in these "Just Accepted" manuscripts.

ACS Publications

Nano Letters is published by the American Chemical Society. 1155 Sixteenth Street N.W., Washington, DC 20036
Published by American Chemical Society. Copyright © American Chemical Society. However, no copyright claim is made to original U.S. Government works, or works produced by employees of any Commonwealth realm Crown government in the course of their duties.

1
2
3
4
5
6
7
8
9
10
11
12
13
14
15
16
17
18
19
20
21
22
23
24
25
26
27
28
29
30
31
32
33
34
35
36
37
38
39
40
41
42
43
44
45
46
47
48
49
50
51
52
53
54
55
56
57
58
59
60

1
2
3
4
5
6
7
8
9
10
11
12
13
14
15
16
17
18
19
20
21
22
23
24
25
26
27
28
29
30
31
32
33
34
35
36
37
38
39
40
41
42
43
44
45
46
47
48
49
50
51
52
53
54
55
56
57
58
59
60

# Intercorrelated in-plane and out-of-plane ferroelectricity in ultrathin two-dimensional layered semiconductor $In_2Se_3$

*Chaojie Cui[1†], Wei-Jin Hu[1,2†*], Xingxu Yan[3], Christopher Addiego[4], Wenpei Gao[3], Yao Wang[5], Zhe Wang[6], Linze Li[3], Yingchun Cheng[5], Peng Li[1], Xixiang Zhang[1], Husam N. Alshareef[1], Tom Wu[1], Wenguang Zhu[6], Xiaoqing Pan[3,4*], Lain-Jong Li[1,7*]*

[1] Physical Sciences and Engineering Division, King Abdullah University of Science and Technology, Thuwal, Jeddah 23955-6900, Kingdom of Saudi Arabia.

[2] Shenyang National Laboratory for Materials Science, Institute of Metal Research (IMR), Chinese Academy of Sciences (CAS), Shenyang 110016, China

[3] Department of Chemical Engineering and Materials Science, University of California - Irvine, Irvine, California 92697, America.

[4] Department of Physics and Astronomy, University of California - Irvine, Irvine, California 92697, America.

[5] Key Laboratory of Flexible Electronics & Institute of Advanced Materials, Jiangsu National Synergetic Innovation Center for Advanced Materials, Nanjing Tech University, Nanjing, Jiangsu 211816, China.

[6] ICQD, Hefei National Laboratory for Physical Sciences at the Microscale, Synergetic Innovation Center of Quantum Information and Quantum Physics, and Key Laboratory of Strongly-Coupled Quantum Matter Physics (CAS), University of Science and Technology of China, Hefei, Anhui 230026, China.

[7] Corporate Research and Chief Technology Office, Taiwan Semiconductor Manufacturing Company, Hsinchu 30075, Taiwan

**KEYWORDS:** 2D materials, $In_2Se_3$, ferroelectric, semiconductor, switchable diode

**ABSTRACT:** Enriching the functionality of ferroelectric materials with visible-light sensitivity and multiaxial switching capability would open up new opportunities for their applications in advanced information storage with diverse signal manipulation functions. We report experimental observations of robust intra-layer ferroelectricity in two-dimensional (2D) van der Waals layered $\alpha$-$In_2Se_3$ ultrathin flakes at room temperature. Distinct from other 2D and conventional ferroelectrics, $In_2Se_3$ exhibits intrinsically intercorrelated out-of-plane and in-plane polarization, where the reversal of the out-of-plane polarization by a vertical electric field also induces the rotation of the in-plane polarization. Based on the in-plane switchable diode effect and the narrow bandgap (~1.3 eV) of ferroelectric $In_2Se_3$, a prototypical non-volatile memory device, which can be manipulated both by electric field and visible light illumination, is demonstrated for advancing data storage technologies.

Conventional ferroelectrics such as barium titanate[1] and lead zirconate titanate (PZT)[2] are large bandgap insulators; hence, their information storage is based predominantly on the capacitor charging and discharging, limiting their applications. Ferroelectrics with a narrow bandgap in visible-light regimes are more desirable because additional operation with light and

1
2
3
4
5
6
7
8
9
10
11
12
13
14
15
16
17
18
19
20
21
22
23
24
25
26
27
28
29
30
31
32
33
34
35
36
37
38
39
40
41
42
43
44
45
46
47
48
49
50
51
52
53
54
55
56
57
58
59
60

convenient read-out with semiconductor features can be incorporated for advanced information storage. Two-dimensional (2D) materials exhibit various functionalities such as high on-off electronic switching, superconductivity[3], ferromagnetism[4], and piezoelectricity[5]. However, 2D ferroelectricity with a narrow bandgap has been rarely reported and its origin still remained unclear. Chang *et al.* demonstrated in-plane (IP) ferroelectricity in a three-dimensional SnTe crystal down to a 1-unit cell thickness[6]. Another known wide-bandgap ferroelectric $CuInP_2S_6$ crystal has been thinned down to 4 nm and demonstrated workable for out-of-plane (OOP) switching[7]. Recently, 2D layered semiconductor $\alpha$-$In_2Se_3$ has been predicted to have both IP and OOP ferroelectric polarization at a monolayer level[8]. Here we report the experimental observations of robust IP and OOP intra-layer ferroelectricity in 2D layered $\alpha$-$In_2Se_3$ at room temperature and fundamental understanding of their antiparallel interlayer polarization. Importantly, the field-induced switching of OPP and IP polarization for $\alpha$-$In_2Se_3$ is proved to be intrinsically intercorrelated. Owing to its ferroelectric nature and the suitable bandgap of ~ 1.3 eV, a lateral two-terminal device based on $\alpha$-$In_2Se_3$ shows a switchable diode effect, where the current can be modulated by electric field and visible light illumination, promising for advancing versatile 2D data storage technologies.

As illustrated in **Fig. 1a,** the $In_2Se_3$ layers were grown on mica substrates by chemical vapor deposition[9]. The $In_2Se_3$ flakes range from few hundred nanometers to several micrometers laterally, with different thicknesses exhibiting different optical contrasts (**Fig. S1**). The atomic force microscopy (AFM) in **Fig. 1b** shows that when the thickness $\geq$ 2 nm the $In_2Se_3$ layers exhibit regular shapes and straight edges, indicating good crystallinity, while those with an apparent thickness <1.3 nm, usually display irregular shapes. From the atomic-resolution scanning transmission electron microscopy (STEM) in **Fig. S2**, we can see it is a mixture of

amorphous and mis-oriented polycrystalline phases, likely resulting from its interaction with underlying mica substrates. Note that various substrates including graphite, silicon and sapphire have been tested for the growth, and mica substrates allow the better growth for $In_2Se_3$. This layer acts as a seed layer for inducing subsequent $In_2Se_3$ growth. Here we consider the layer grown on top of the seed layer as the monolayer. It is known that bulk $In_2Se_3$ exists in various crystalline phases including $\alpha$ and $\beta$, and there is a phase transformation between $\alpha$ and $\beta$ phases occurring at ~ 200 $^{o}$C[10, 11]. Thus, the cooling rate after the growth (at 660 $^{o}$C) is critical for obtaining $\alpha$ phase (see **Methods**), which is predicted to be ferroelectric.[8] Fig. 1c shows the Raman spectra of the as-grown $In_2Se_3$ flakes, where the three peaks at ~103, 170, 204 cm$^{-1}$ observed in the sample with slow cooling (0.1 $^{o}$C/min) are attributed to $A_1$ (LO + TO), $A_1$ (TO) and $A_1$ (LO) phonon modes of $In_2Se_3$.[9, 11] It is reported that there would be a blue shift in lattice phonon modes for $\beta$-$In_2Se_3$ compared with that of $\alpha$-$In_2Se_3$ due to the smaller lattice constant of $\beta$-$In_2Se_3$, and the relative peak intensity of A1 (TO) phonon mode for $\beta$-$In_2Se_3$ is much weaker than that of $\alpha$-$In_2Se_3$.[11, 12] In our case, we don't see obvious Raman shift between the quick cooling and slow cooling samples, because both samples are the mixtures of $\alpha$- and $\beta$-$In_2Se_3$. The minor peak at ~170 cm$^{-1}$ for the quick cooling sample indicates that it is dominated by $\beta$ phase[11, 12], while the strong intensity of this peak for the slow cooling sample suggests that the portion of $\alpha$-$In_2Se_3$ flakes significantly increases in the slow cooling process.

**Fig. 1d** displays the selected area electron diffraction (SAED) patterns from two regions of the $In_2Se_3$ sample obtained with slow cooling. The left SAED was acquired from a monolayer as shown in the low-magnification TEM image in the inset, which matches with $\alpha$-$In_2Se_3$ along the [0001] axis. The right SAED from another thicker flake (12 nm thick) is assigned to $\beta$-$In_2Se_3$, where the additional diffraction spots along the $[1\bar{1}00]$ direction indicates the existence of

superstructures[11, 13, 14]. We note that $\alpha$-$In_2Se_3$ is typically observed in thin flakes (e.g. less than around 10L) but rarely found in thicker flakes. **Fig. 1e** shows the atomic-resolution STEM image of a monolayer $\alpha$-$In_2Se_3$, confirming the success in growing $\alpha$-$In_2Se_3$ flakes. Because four different atomic configurations have been proposed for $\alpha$-phase[8, 14], We simulated diffraction patterns based on kinematic diffraction for these various configurations (**Fig. S3**). The comparison of experimental and simulated patterns allows us to conclude that $\alpha$-$In_2Se_3$ exists in the FE-ZB' configuration, agreeable with the theoretical prediction[8].

To study the spontaneous ferroelectric polarization, we investigated the as-grown $\alpha$- and $\beta$-$In_2Se_3$ thin flakes on mica substrates by piezoresponse force microscopy (PFM) (see **Methods**). The PFM amplitude reflects the magnitude of the local piezoelectric response, and the phase indicates the direction of the ferroelectric polarization. As expected, no phase contrast difference is observed for $\beta$-$In_2Se_3$ in both the IP and OOP directions since it is not a ferroelectric phase (**Fig. S4). Fig. 2a** shows the topographic image of the randomly selected triangle $\alpha$-$In_2Se_3$ flakes with the thickness from 2 nm to 6 nm. The OOP PFM images for these flakes are shown in **Fig. S5a** (amplitude) and **S5b** (phase) and the corresponding IP PFM images are shown in **Figs. 2b** (amplitude) and **2c** (phase). We observe from **Figs. 2b** and **2c** that the single ferroelectric domain is formed within each terrace. Although single domain state is rarely achieved for traditional ferroelectric without applying an electric field, it is favorable when the depolarizing field is small and fully compensated, which is likely the case of $\alpha$-$In_2Se_3$ because the IP polarization is larger than OOP polarization. The high carrier concentration of $\alpha$-$In_2Se_3$ could also neutralize the boundary polarization charges, making it possible for the formation of single domain state[15]. This is different from $CuInP_2S_6$, where OOP polarization dominates and thus the domain walls easily form even for ultrathin films[7].

1 2 3 4 5 6 7 8 9 10 11 12 13 14 15 16 17 18 19 20 21 22 23 24 25 26 27 28 29 30 31 32 33 34 35 36 37 38 39 40 41 42 43 44 45 46 47 48 49 50 51 52 53 54 55 56 57 58 59 60

**Fig. 2c** also indicates that there exist two IP polarization directions with opposite phase contrasts in $\alpha$-$In_2Se_3$ and such a phase contrast is thickness-dependent. Specifically, the phase of a 2 nm flake is ~$120^o$, while it is ~ -$60^o$ for a 3 nm flake, and it reverts to ~$120^o$ for a 4 nm flake. The analysis for the IP phase contrast dependency on layer number is detailed in **Fig. S6** and the results are summarized in **Fig. 2d.** Since the seed layer is poorly crystallized, we only study the ferroelectricity for the flakes $\geq$ 2 nm (1L). In brief, the obvious odd-even effect is observed for the flakes ranging from 1L to 6L. The anti-aligned IP polarization should generally result in zero polarization for the flakes with an even layer number (cancellation of opposite polarizations). However, PFM measurement is most sensitive to surface polarization, and a working depth of several nanometers has been reported for PZT films[16, 17]. The working depth could be even smaller for 2D $In_2Se_3$ partially due to the weak van der Waals interactions between each layer. Hence, the odd-even effect could still be observed. In addition, the OOP phase mapping also shows the similar behaviors although the OOP polarization is several tens of times smaller than the IP polarization[8]. Such a layer-dependent odd-even ferroelectric effect has been predicted for monolayer Group-IV monochalcogenides[18], and our results have proved the validity for the first time in 2D materials. Our density functional theory calculations for $\alpha$-$In_2Se_3$ bilayer also indicate that both the IP and OOP polarizations favor the anti-parallel stacking (**Fig. S7)**. The scanning electron diffraction (SED) is further used to study the interlayer antiparallel-polarization phenomenon in $\alpha$-$In_2Se_3$. When the electron probe scan through the sample, it can be shifted by the local electric field or diffracted by the local atomic structure[19], allowing to map the local projected electric field. **Fig. 2e** shows the high-angle annular dark field (HAADF) STEM image of the region probed with SED. Based on the image intensity from the z-contrast in **Fig. 2f** and low-mag STEM image in **Fig. S8**, a 2L to 3L boundary of $\alpha$-$In_2Se_3$ could be identified. The map

1
2
3
4
5
6
7
8
9
10
11
12
13
14
15
16
17
18
19
20
21
22
23
24
25
26
27
28
29
30
31
32
33
34
35
36
37
38
39
40
41
42
43
44
45
46
47
48
49
50
51
52
53
54
55
56
57
58
59
60

of electric field projected along the [0001] zone axis of $In_2Se_3$ is shown in **Fig. 2g**, where each vector shows the direction of the local electric field, with its magnitude indicating the field strength. We identified a clear electric field switching from the $[\bar{1}010]$ to the $[10\bar{1}0]$ direction within the $In_2Se_3$ basal plane from 2L to 3L. The line profile of mean electric field projected along the X direction in **Fig. 2h** manifests that the electric field is clearly reversed in X direction and has a small reversal in Y direction.

Ferroelectric materials should be able to respond to the applied electric field; *i.e.*, the polarization can be manipulated by the electric field. To explore the polarization switching, $\alpha$-$In_2Se_3$ flakes were transferred onto the Au (or Pt)-coated Si substrate. The OOP (**Fig. 3b**) and IP (**Fig. 3c**) phase images acquired after writing two square patterns with opposite tip voltages (-7 V and +6 V) demonstrate that polarization direction can be controlled by the external bias. More importantly, the IP phase changes simultaneously with the OOP phase, indicating that the IP polarization is intercorrelated with the OOP polarization. According to the theoretical calculations,[8] this unique IP and OOP intercorrelation could intrinsically originate from electric field-induced lateral movement of the central Se atomic layer in the FE-ZB' configuration (Fig. 3a). Other 2D ferroelectrics only exhibit one polarization component (e.g. IP for SnTe, and OOP for $CuInP_2S_6$). The intercorrelated polarization is beneficial for new memory devices switchable by a perpendicular or horizontal electric field. Meanwhile, the phase contrast of the written domains fades with time but is still identifiable after 2 h (**Fig. S9**), suggesting the good stability of the written domains. The maximum time period of the identifiable phase contrast is ~ 10 h. Together with the domain writing, the local piezoelectric loops of this 6 nm thick flake in **Fig. 3d** display a butterfly-like voltage dependent amplitude loop and the sharp change in phase up to $180^o$, typical for ferroelectrics. Note that similar hysteresis loops could also be observed in some

non-ferroelectrics, due to the surface electrostatic effect between the tip and surface charges or ion movement under high external electric field[20]. The deposition of a top conducting electrode will produce a homogeneous electric field to avoid local charge/ion accumulation, largely alleviate these effects. Fig. 3e shows that butterfly-like amplitude loop and sharp phase hysteresis loop were still obtained for an $\alpha$-$In_2Se_3$ flake with a top Au electrode (see methods). Thus, these possible artifacts are excluded. Compared with that of the bare $In_2Se_3$ flake, the amplitude/phase loop acquired on $In_2Se_3$ flake with a top Au pad is more asymmetric and show larger coercivity, which could be attributed to the dead layer between $In_2Se_3$ and the top gate electrode induced during the Au deposition. The switchable polarization for more flakes is included in **Fig. S10**.

To show the possible application of ferroelectric $In_2Se_3$ as non-volatile memory element, we investigated the transport properties of thin $In_2Se_3$ flakes in the OOP direction by performing conducting atomic force microscope (CAFM). **Fig. 4a** is the current mapping of a 6 nm thick $In_2Se_3$ flake after writing with -6V and +6V stripes respectively**,** which clearly shows high and low current states corresponding to opposite polarization states. The typical local *I-V* curves in **Fig. 4b** demonstrates that for the -6V written region the current changes by more than four orders upon the polarization reversal, comparable with the resistive switching observed for other traditional ferroelectric oxides[20]. The non-linear feature of the *I-V* curves especially for the high current state suggests that the transport is dominated by the interfacial barriers between the $\alpha$-$In_2Se_3$ and the two electrodes, where the metal/ferroelectric/metal sandwiched structure could be considered as back-to-back Schottky diodes with the Schottky barrier height varied with the polarization direction[20,21].

1
2
3
4
5
6
7
8
9
10
11
12
13
14
15
16
17
18
19
20
21
22
23
24
25
26
27
28
29
30
31
32
33
34
35
36
37
38
39
40
41
42
43
44
45
46
47
48
49
50
51
52
53
54
55
56
57
58
59
60

Leveraging on the concurrent ferroelectric and semiconductor properties of $\alpha$-$In_2Se_3$, a lateral resistive memory device (Au/$\alpha$-$In_2Se_3$/Au as illustrated in **Fig. 4c** and **Fig. S11**) based on the IP polarization is further constructed. **Fig. 4e** shows the typical *I-V* curves for the device performed in the range of $\pm$10 V. The arrows in the figure denote the voltage sweep directions. The *I-V* curve with distinct hysteresis behaviors shows a resistive switching (on/off ratio of ~ 10). Two *I-V* segments in the range of $\pm$4V are replotted by red and blue solid lines, respectively, demonstrating obvious opposite rectifying features. This switchable diode effect upon the IP polarization reversal totally differs from that of the common ferroelectric capacitors which rely on the OOP polarization reversal[21]. **Fig. 4d** displays the schematic band alignment of the lateral device. Due to the built-in electric field of the ferroelectric layer, the ferroelectric polarization can enhance the Schottky barrier of one interface while reducing the barrier of the opposite interface, leading to an asymmetric transport behavior as shown in **Fig. 4e**. Detailed *I-V* curves with various biases are discussed in **Fig. S11**. In addition to the electric field, **Fig. 4e** shows that the $\alpha$-$In_2Se_3$ planar device is also sensitive to the visible light due to the semiconducting nature of $\alpha$-$In_2Se_3$, which remains semiconducting with a measured bandgap of ~ 1.3 eV even as thin as a bilayer (**Fig. S12**). A multi-functional memory device with four resistive memory states switchable with electric field and light illumination is then realized, showing potential for advanced data storage technologies. Whereas for $\beta$-$In_2Se_3$ based device (**Fig. S13**), we do not observe resistive switching behavior but only the light response.

In summary, robust layer dependent intra-layer ferroelectricity has been experimentally demonstrated in 2D semiconducting $\alpha$-$In_2Se_3$. The tangled switching behavior of the IP and OOP polarization in $\alpha$-$In_2Se_3$ distinguishes it from other 2D and conventional ferroelectrics. A simple

1 2 3 4 5 6 7 8 9 10 11 12 13 14 15 16 17 18 19 20 21 22 23 24 25 26 27 28 29 30 31 32 33 34 35 36 37 38 39 40 41 42 43 44 45 46 47 48 49 50 51 52 53 54 55 56 57 58 59 60

device taking the advantage of both the switchable polarization and the visible light absorption exhibits memristive behavior, promising for applications in 2D nanoelectronics for data storage. Our results broaden the functionalities of 2D materials and suggest new opportunities for van der Waals heterostructures.

**Notes:** When preparing the manuscript, we notice a recent paper by Zhou, Y., *et al* [22] showing the experimental observation of OOP piezoelectricity and ferroelectricity of thick $In_2Se_3$. Here, we show a fundamentally important layer dependent ferroelectricity, and intercorrelated OP and IP polarization switching of ultrathin $\alpha$-$In_2Se_3$. Furthermore, a switchable diode effect that can be controlled by both the electric field and visible light illumination on a two terminal device has been confirmed, which promises potential applications such as memory and optical sensors.

## Methods

*Growth of 2D layered $In_2Se_3$.* The 2D layered $In_2Se_3$ was synthesized on mica substrates by chemical vapor deposition method using Se and $In_2O_3$ powders as the precursors and the $H_2$/Ar mixture as the carrier gas.[9] The boat filled with 0.1 g $In_2O_3$ was placed in the center of the furnace and the boat full of Se was in the upstream. The mica without any special treatment was placed in the downstream about 15 cm away from the boat of $In_2O_3$. The temperature of Se and $In_2O_3$ were heated to 330 and 660 $^{o}$C respectively in 30 min and were kept for 30 min for the growth of 2D layered $In_2Se_3$ under a pressure of 500 torrs in the atmosphere of 30 ml/min $H_2$ and 90 ml/min Ar. After synthesis, the system was cooled down to room temperature in about 20 min for fast cooling process or 3 days for the slow cooling process, respectively.

*Transfer of $In_2Se_3$ from mica to target substrates.* The transfer of $In_2Se_3$ was assisted with a poly(methyl methacrylate) (PMMA) transfer supporting layer. The PMMA was spin-coated on

1
2
3
4
5
6
7
8
9
10
11
12
13
14
15
16
17
18
19
20
21
22
23
24
25
26
27
28
29
30
31
32
33
34
35
36
37
38
39
40
41
42
43
44
45
46
47
48
49
50
51
52
53
54
55
56
57
58
59
60

the surface of the $In_2Se_3$ samples grown on mica and then baked at 180 $^oC$ for 2 min. After ultrasonic in water for 2 min, the PMMA/$In_2Se_3$ film was peeled off from the mica with the assistance of water. Then the PMMA/$In_2Se_3$ film was fished by the target substrates, such as silicon wafer or TEM grid.

*Raman and AFM measurement.* The Raman measurement was performed using an excitation laser of 532 nm (WITec alpha 300 confocal Raman microscopy). The AFM measurement was performed by Cypher ES - Asylum Research Oxford Instruments.

*Electron Microscopy observation and analysis.* TEM and SAED were carried out using a JEOL JEM-2100F TEM at the accelerating voltage of 200 kV. High resolution STEM imaging was acquired using the Nion UltraSTEM 200 at University of California - Irvine, equipped with C3/C5 corrector and high-energy resolution monochromated EELS system (HERMES). The instrument was operated at 60kV to avoid knock-on damage. The semi-angle of the probe-forming aperture was about 30 mrad and the beam current was about 30 pA. The inner and outer cut-off semi-angles of the HAADF detector were about 70 and 200 mrad, respectively, and the acquisition time was chosen to be 32 μs per pixel. Scanning electron diffraction was carried out on a JEOL JEM-300CF S/TEM equipped with both imaging and probe forming aberration correctors. An electron probe of the size of ~1 Å was formed by converging the electron beam at a convergence semi-angle of ~18 mrad. The electron accelerating voltage was 80 kV. Convergent beam electron diffraction patterns (CBED) were taken at each scanning point using Gatan OneView camera at the speed of 200 frames per second. The penetrating electron beam will be shifted by the local electric field along its path through the sample[19]. By measuring the shift of the center of weight (CoW) of the intensity in each CBED pattern, the electric field can

1
2
3 be quantified. The detailed description of scanning electron diffraction can be found in supplementary materials.

*Ferroelectric characterization.* Piezoresponse force microscopy and conducting atomic force microscopy measurements were performed using a commercial atomic force microscope (Asylum Research MFP-3D) with Pt/Ir-coated Si cantilever tips and diamond-coated Si cantilever tips, respectively. In typical PFM measurements, an ac voltage of amplitude of 1000 mV was applied on the tip. The OOP and IP piezoelectric signals are acquired at a contact resonance frequency of ~ 56 kHz and ~172 kHz respectively in DART (dual a.c. resonance tracking) mode[23]. PFM were also performed on transferred $In_2Se_3$ flakes with top Au electrodes (2 μm in diameter and 20 nm in thickness), which were fabricated by standard E-beam lithography writing, followed by Au film deposition through E-beam evaporation at a growth rate of 0.1 nm/s, and finally by standard lift-off process. For the local electric measurements, the bias voltage was applied on the sample. For CAFM mapping, a dc bias voltage of 0.5 V was applied.

*Electric characterizations. I-V* curves of planar devices were investigated by a Keithley 4200 semiconductor analyzer connected to a probe station at room temperature. A visible light LED with an intensity of ~ 8 $mW/cm^2$ was used for the light response test.

*Density functional theory calculation.* First principles calculations based on density functional theory (DFT) were performed using the Vienna Ab Initio Simulation Package[24]. The exchange and correlation functionals were treated using the PBE[25] parametrization of GGA with the kinetic energy cutoff set to 550 eV. A 12 × 12 × 1 k-meshes were used for the Brillouin zone sampling. For the band structure calculations, the hybrid functional of Hyed-Scuseria-Ernzerhof

(HSE06)[26] was employed. A vacuum thickness of 20 Å is adopted to ensure that the interactions between the layers are negligible. The van der Waals interaction (optB88-vdW, Ref 27) was adopted in the structure relaxation steps. Optimized atomic structures were achieved when forces on all the atoms have declined to less than 0.005 eV/Å.

## ASSOCIATED CONTENT

**Supporting Information**. The optical images, the STEM images and diffraction patterns, other PFM images, density functional calculations, and detailed electric characterizations of devices are given in this section. This material is available free of charge via the internet.

## AUTHOR INFORMATION

**Corresponding Authors**

*Email: *weijin.hu@kaust.edu.sa*; *xiaoqinp@uci.edu*; *lance.li@kaust.edu.sa*

**Author Contributions**

[†] C.J.C. and W.J.H. contributed equally to this work.

**Notes**

The authors declare no competing financial interest.

## ACKNOWLEDGMENT

L.J.L. thanks the support from King Abdullah University of Science and Technology (Saudi Arabia). The work at University of California - Irvine was supported by the Department of Energy (DOE), Office of Basic Energy Sciences, Division of Materials Science and Engineering, under Grant under Grant No. DE-SC0014430, and the Irvine Materials Research Institute (IMRI). We would like to thank Dr. Toshi Aoki from IMRI for his help on S/TEM experiments.



ACS Paragon Plus Environment

1
2
3
4
5
6
7
8
9
10
11
12
13
14
15
16
17
18
19
20
21
22
23
24
25
26
27
28
29
30
31
32
33
34
35
36
37
38
39
40
41
42
43
44
45
46
47
48
49
50
51
52
53
54
55
56
57
58
59
60

REFERENCES

1. Choi, K. J.; Biegalski, M.; Li, Y. L.; Sharan, A.; Schubert, J.; Uecker, R.; Chen, Y. B.; Pan, X. Q.; Gopalan, V.; Chen, L. Q.; Schlom, D. G. & Eom, C. B. *Science* **2004,** *306,* 1005–1009.

2. Scott, J. F. *Science* **2007,** *315,* 954–959.

3. Zhang, T.; Cheng, P.; Li, W. J.; Sun, Y. J.; Wang, G.; Zhu, X. G.; He, K.; Wang, L. L.; Ma, X. C.; Chen, X.; Wang, Y. Y.; Liu, Y.; Lin, H. Q.; Jia, J. F. & Xue, Q. K. *Nat. Phys.* **2010**, *6,* 104–108.

4. Gong, C.; Li, L.; L, Z. L.; J, H. W.; Stern, A.; Xia, Y.; Cao, T.; Bao, W.; Wang, C. Z.; Wang, Y.; Qiu, Z. Q.; Cava, R. J.; Louie, S. G.; Xia, J. & Zhang, X. *Nature* **2017**, *546,* 265–269.

5. Wu, W. Z.; Wang, L.; Li, Y. L.; Zhang, F.; Lin, L.; Niu, S. M.; Chenet, D.; Zhang, X.; Hao, Y. F.; Heinz, T. F.; Hone, J. & Wang, Z. L. *Nature* **2014,** *14,* 470−474.

6. Chang, K.; Liu, J. W.; Lin, H. C.; Wang, N.; Zhao, K.; Zhang, A. M.; Jin, F.; Zhong, Y.; Hu, X. P.; Duan, W. H.; Zhang, Q. M.; Fu, L.; Xue, Q. K.; Chen, X. & Ji, S. H. *Science* **2016,** *353,* 274−278.

7. Liu, F. C.; You, L.; Seyler, K. L.; Li, X. B.; Yu, P.; Lin, J. H.; Wang, X. W.; Zhou, J. D.; Wang, H.; He, H. Y.; Pantelides, S. T.; Zhou, W.; Sharma, P.; Xu, X. D.; Ajayan, P. M.; Wang, J. L. & Liu, Z. *Nat. Commun.* **2016,** *7,* 12357.

8. Ding, W. J.; Zhu, J. B.; Wang, Z.; Gao, Y. F.; Xiao, D.; Gu, Y.; Zhang, Z. Y. & Zhu, W. G. *Nat. Commun.* **2017,** *8,* 14956.

9. Feng, W.; Zheng, W.; Gao, F.; Chen, X. S.; Liu, G. B.; Hasan, T.; Cao, W. W. & Hu, P. A. *Chem. Mater.* **2016,** *28,* 4278−4283.

10. Kim, H. G.; Min, I. S. & Kim, W. T. *Solid State Commun.* **1987,** *64,* 819−822.

11. Tao, X. & Gu, Y. *Nano Lett.* **2013,** *13,* 3501−3505.

1
2
3
4
5
6
7
8
9
10
11
12
13
14
15
16
17
18
19
20
21
22
23
24
25
26
27
28
29
30
31
32
33
34
35
36
37
38
39
40
41
42
43
44
45
46
47
48
49
50
51
52
53
54
55
56
57
58
59
60

12. Ke, F.; Liu, C. L.; Gao, Y.; Zhang, J. K.; Tan, D. Y.; Han, Y. H.; Ma, Y. Z.; Shu, J. F.; Yang, W. G.; Chen, B.; Mao, H. K.; Chen, X. J. & Gao, C. X. *Appl. Phys. Lett.* **2014,** *104,* 212102.

13. Lin, M.; Wu, D.; Zhou, Y.; Huang, W.; Jiang, W.; Zheng, W. S.; Zhao, S. L.; Jin, C. H.; Guo, Y. F.; Peng, H. L. & Liu, Z. F. *J. Am. Chem. Soc.* **2013,** *135,* 13274−13277.

14. Ye, J. P.; Soeda, S.; Nakamura, Y. & Nittono, O. *Jpn. J. Appl. Phys.* **1998,** *37,* 4264−4271.

15. Kooi, B. J. & Noheda, B. *Science*, **2016,** *353,* 221-222.

16. Kalinin, S. V. & Gruverman, A. Scanning Probe Microscopy: Electrical and Electromechanical Phenomena at the Nanoscale, Chapt. 6 (New York: Springer, 2007).

17. Ganpule, C. S.; Nagarajan, V.; Hill, B. K.; Roytburd, A. L.; Williams, E. D.; Ramesh, R.; Alpay, S. P.; Roelofs, A.; Waser, R. & Eng, L. M. *J. Appl. Phys.* **2002,** *91,* 1477.

18. Fei, R.; Kang, W. & Yang, L. *Phys. Rev. Lett.* **2016,** *117,* 097601.

19. Shibata, N.; Findlay, S. D.; Kohno, Y.; Sawada, H.; Kondo, Y. & Ikuhara, Y. *Nat. Phys.* **2012,** *8,* 611−615.

20. Kim, D. J.; Paudel, T. R.; Lu, H. D.; Burton, J. D.; Connell, J. G.; Tsymbal, E. Y.; Ambrose Seo, S. S. & Gruverman, A. *Adv. Mater.* **2014,** *26,* 7660−7665.

21. Yi, H. T.; Choi, T.; Choi, S. G.; Oh, Y. S. & Cheong, S. W. *Adv. Mater.* **2011,** *23,* 3403−3407.

22. Zhou, Y.; Wu, D.; Zhu, Y. H.; Cho, Y. J.; He, Q.; Yang, X.; Herrera, K.; Chu, Z. D.; Han, Y.; Downer, M.; Peng, H. L. & Lai, K. J. *Nano lett.* **2017,** *17,* 5508−5513.

23. Rodriguez, B. J.; Callahan, C.; Kalinin, S. V. & Proksch, R. *Nanotechnology* **2007,** *18,* 475504.

24. Kresse, G. & Furthmüller, J. *Phys. Rev. B* **1996,** *54,* 11169–11186.

25. Perdew, J. P.; Burke, K. & Ernzerhof, M. *Phys. Rev. Lett.* **1996,** *77,* 3865–3868.

26. Krukau, A. V.; Vydrov, O. A.; Izmaylov, A. F. & Scuseria, G. E. *J. Chem. Phys.* **2006,** *125,* 224106.

27. Klimeŝ, J.; Bowler, D. R. & Michaelides, A. *J. Phys. Condens. Matter* **2010,** *22,* 022201.

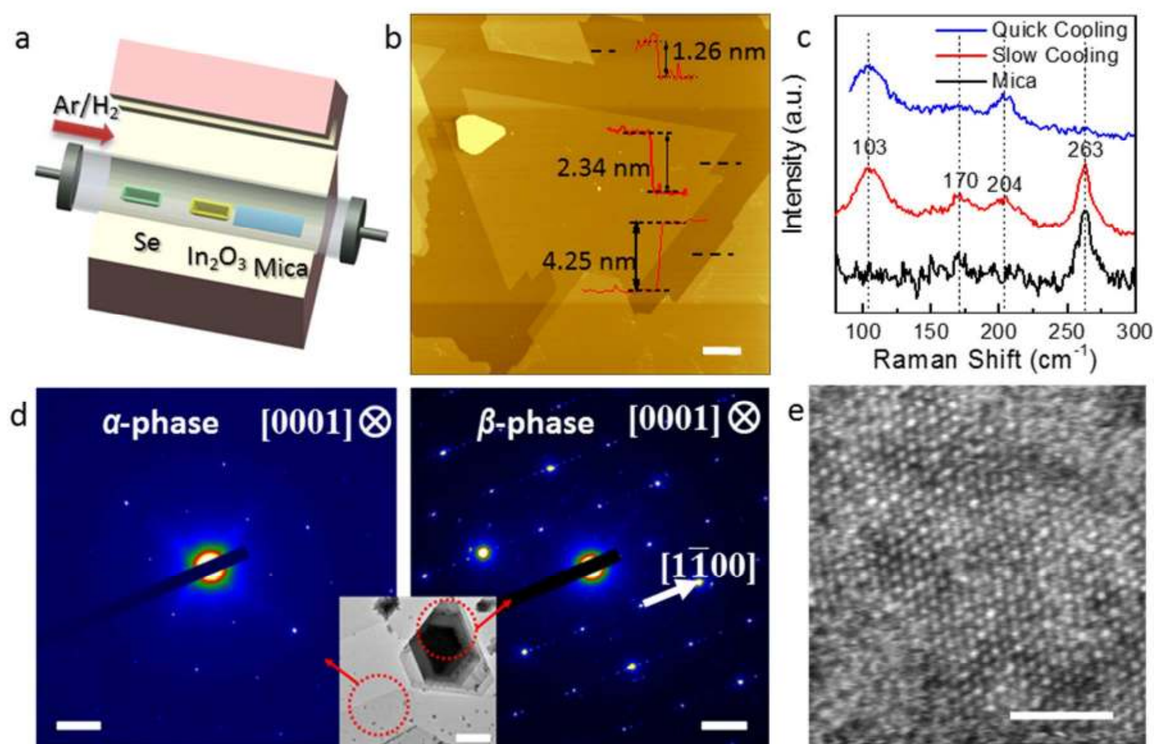


**Figure 1. Synthesis & structure characterization of 2D $In_2Se_3$. a.** Schematic illustration of the growth process of 2D $In_2Se_3$ with Se and $In_2O_3$ as the precursors and mica as the substrate. **b.** AFM image and the corresponding height profiles of $In_2Se_3$ sheets with the thicknesses ~1.3-4.3 nm. The scale bar is 1 μm. **c.** Raman spectra of $In_2Se_3$ and mica respectively with the 532 nm laser excitation. **d.** SAED patterns of *α*- and *β*- $In_2Se_3$ taken in the regions indicated in the TEM image in the inset, where the scale bar for SAED and TEM is 2 $nm^{-1}$ and 500 nm respectively. **e.** Atomic-resolution STEM image of a monolayer *α*-$In_2Se_3$. The scale bar is 2 nm.

1
2
3
4
5
6
7
8
9
10
11
12
13
14
15
16
17
18
19
20
21
22
23
24
25
26
27
28
29
30
31
32
33
34
35
36
37
38
39
40
41
42
43
44
45
46
47
48
49
50
51
52
53
54
55
56
57
58
59
60

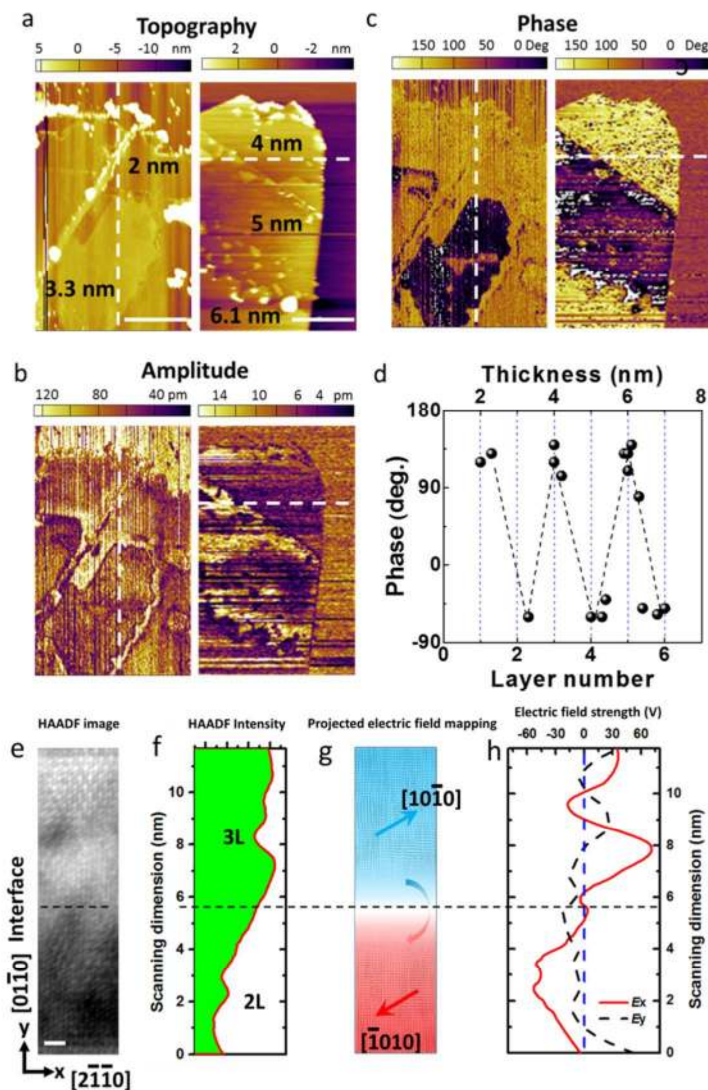


**Figure 2. PFM investigation of the as-grown $In_2Se_3$ on mica. a.** AFM image of typical thin flakes with the thicknesses from 2 to 6 nm. The scale bars is 1 μm. **b and c**, The corresponding IP PFM images (b. amplitude; c. phase). **d.** Statistics of the thickness-dependent IP phase (1L-6 L) from different locations. **e.** STEM-HAADF image showing the region from 2L (lower) to 3L (upper), where scanning electron diffraction was performed. The X-Y axes are indicated in bottom left, where X is along the $[2\bar{1}\bar{1}0]$ direction and Y is along the $[01\bar{1}0]$ direction of α-$In_2Se_3$. The scale bar is 1 nm. **f.** Average intensity profile of HAADF image along the Y

1
2
3 direction in e. **g.** Projected electric field mapping in the same region as f. The major direction of
4
5
6 electric field in upper and lower regions are close to $[10\bar{1}0]$ and $[\bar{1}010]$ directions, respectively.
7
8 **h.** Line profiles of the X- and Y- components of the mean projected electric field strength along
9
10 X-direction and Y-direction, as indicated by $E_x$ and $E_y$, respectively.
11
12
13
14
15
16
17
18
19
20
21
22
23
24
25
26
27
28
29
30
31
32
33
34
35
36
37
38
39
40
41
42

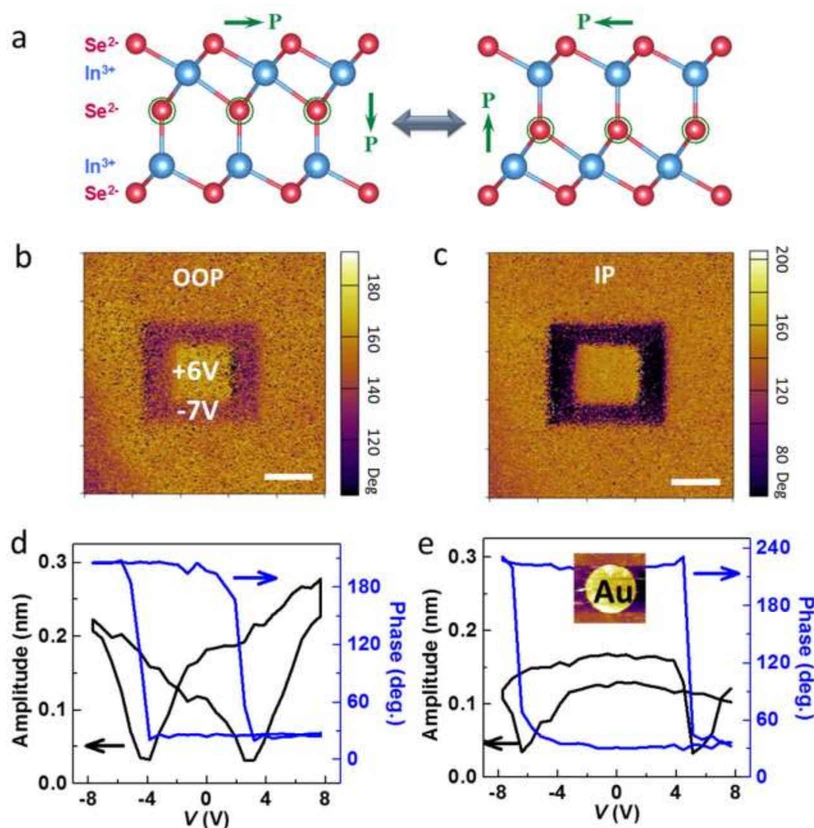


43 **Figure 3. Ferroelectric switching of a 6 nm thin $In_2Se_3$ flake transferred onto the Au/Si**
44
45 **substrate. a.** schematic model of IP and OOP switching coupling. **b.** OOP phase image and **c.**
46
47 the corresponding IP phase image of a 6 nm thick $In_2Se_3$ flake acquired immediately after
48
49
50 writing two square patterns with a size of 2 μm and 1 μm by applying -7 V and +6 V voltages
51
52 consecutively. The scale bar is 1 μm. **d and e.** Local ferroelectric switching loops without and
53
54
55 with an Au top electrode, respectively.
56
57
58
59
60

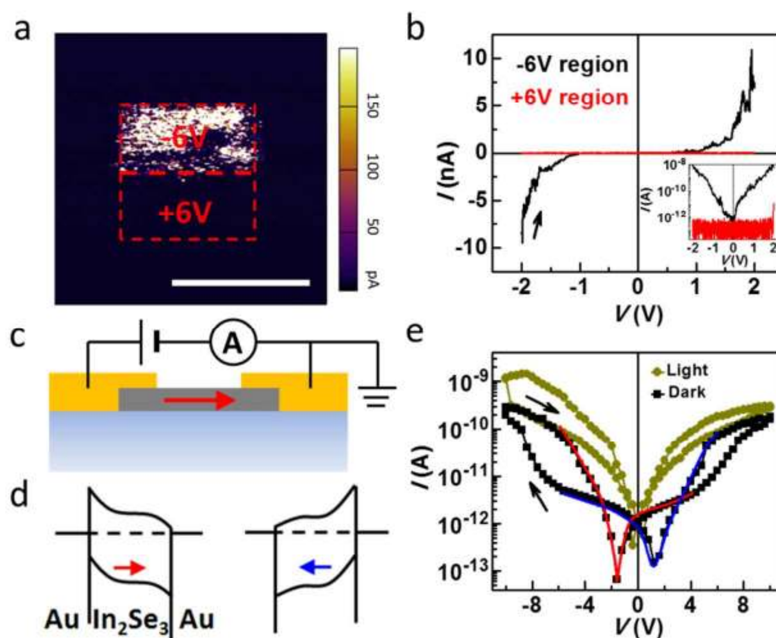


**Figure 4. Electrically controlled conducting behavior of $In_2Se_3$. a.** CAFM mapping for a 6 nm thick flake of $\alpha$-$In_2Se_3$ transferred onto a Pt/Si substrate. The mapping was collected after writing with +6 V/-6 V stripes (1 μm × 0.5 μm). The scale bar is 1 μm. **b.** Local *I-V* curves measured in +6 V and -6 V switched regions. Inset, same data in log scale. **c and d.** Schematic planar device structure and the polarization direction dependent band alignment. The planar device on mica was built with an as-grown $\alpha$-$In_2Se_3$ thin flake (~13 nm) bridged by two Au electrodes. **e.** *I-V* curve of the planar $In_2Se_3$ device. The red and blue solid lines are used to guide the eyes.

1
2
3
4
5
6
7
8 TOC:
9
10
11
12
13
14
15
16
17
18
19
20

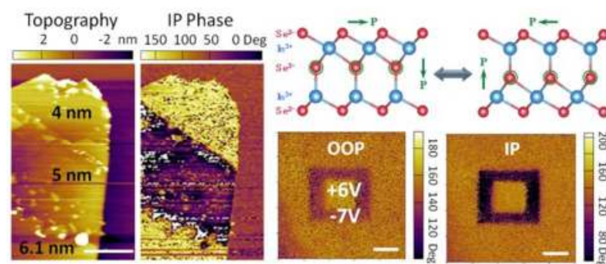


21
22
23
24
25
26
27
28
29
30
31
32
33
34
35
36
37
38
39
40
41
42
43
44
45
46
47
48
49
50
51
52
53
54
55
56
57
58
59
60